

# Complex paths for regular-to-chaotic tunneling rates

Normann Mertig,<sup>1,2</sup> Steffen Löck,<sup>1,2</sup> Arnd Bäcker,<sup>1,2</sup> Roland Ketzmerick,<sup>1,2</sup> and Akira Shudo<sup>2,3</sup>

<sup>1</sup>*Institut für Theoretische Physik, Technische Universität Dresden, 01062 Dresden, Germany*

<sup>2</sup>*Max-Planck-Institut für Physik komplexer Systeme, Nöthnitzer Straße 38, 01187 Dresden, Germany*

<sup>3</sup>*Department of Physics, Tokyo Metropolitan University, Minami-Osawa, Hachioji, Tokyo 192-0397, Japan*

(Dated: June 15, 2018)

In generic Hamiltonian systems tori of regular motion are dynamically separated from regions of chaotic motion in phase space. Quantum mechanically these phase-space regions are coupled by dynamical tunneling. We introduce a semiclassical approach based on complex paths for the prediction of dynamical tunneling rates from regular tori to the chaotic region. This approach is demonstrated for the standard map giving excellent agreement with numerically determined tunneling rates.

PACS numbers: 05.45.Mt, 03.65.Sq

Tunneling is a fundamental manifestation of quantum mechanics. Its basic features are established in standard textbooks [1, 2] for particles confined by one-dimensional energy barriers: While the particle is classically trapped, it can escape quantum mechanically if the energy barrier is finite. This process typically exhibits an exponential decay  $\exp(-\gamma t)$ , which is characterized by the tunneling rate  $\gamma$ . This rate describes the inverse life-time of the confined state and captures the relevant information of the tunneling process. Since time-independent one-dimensional systems have integrable dynamics, the tunneling rates through the energy barrier can be computed from complex WKB-paths in the classically forbidden region [1–4]

$$\gamma \propto \exp\left(-\frac{2 \operatorname{Im} \mathcal{S}}{\hbar}\right). \quad (1)$$

Here, the imaginary part of the action  $\mathcal{S} = \int p dq$ , which increases with the width and the height of the barrier, is divided by Planck's constant  $\hbar = 2\pi\hbar$ . In the semiclassical limit this ratio increases and tunneling vanishes exponentially.

In contrast to one-dimensional potential wells, many systems of physical relevance have non-integrable Hamiltonians such as driven atoms and molecules [5–7], cold-atom systems [8, 9], optical as well as microwave cavities [10–14], and nano-wires [15]. These systems generically have a mixed phase space in which classically disjoint regions of regular and chaotic motion coexist. Quantum mechanical transitions between such regions are called dynamical tunneling [16, 17]. In the above systems dynamical tunneling is the key to understanding life-times and decay channels of long-lived states associated to a regular region. Furthermore, dynamical tunneling has important consequences for the structure of eigenfunctions [18, 19] and spectral statistics [20–23] in mixed systems. Due to this broad interest a lot of effort has been made to investigate dynamical tunneling experimentally [8–11] and theoretically [24–38].

In this paper we derive a semiclassical prediction of dynamical tunneling rates  $\gamma$  for the ubiquitous situa-

tion of regular-to-chaotic tunneling. The focus is on the experimentally relevant regime, in which direct tunneling to the chaotic region dominates. We generalize the WKB-formula, Eq. (1), to mixed systems by unifying the semiclassical time evolution method of complex paths [28] with the fictitious integrable system approach [36]. This demonstrates that direct regular-to-chaotic tunneling rates are determined by complex paths, which connect regular tori to the boundary between the regular and the chaotic region, see Fig. 1. This approach is successfully applied to the standard map.

In the following we explain our semiclassical complex path approach to dynamical tunneling rates for mixed systems. For simplicity we restrict the presentation to

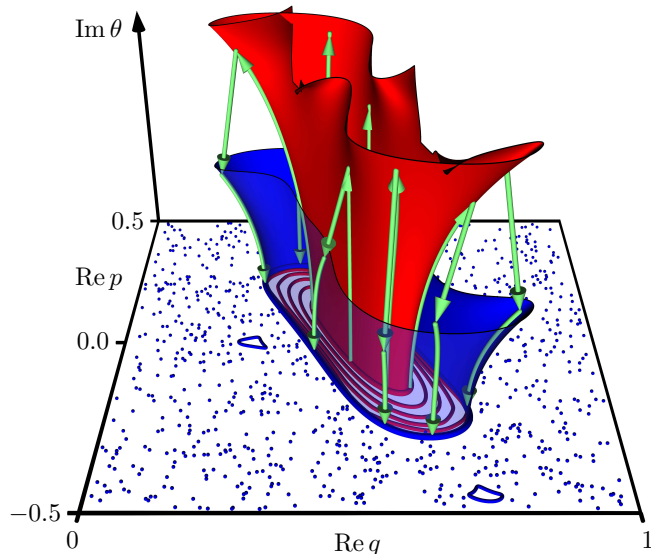


FIG. 1. (color online) Dominant complex paths (green arrows) for the direct regular-to-chaotic tunneling rate  $\gamma_1$  of the standard map at  $\kappa = 2.9$  and  $\hbar = 1/50$ . The initial (inner red) torus and the final (outer blue) torus of the fictitious integrable system emerge from the real classical phase space.

time-periodic quantum systems, described by a time evolution operator  $\hat{U}$  over one period of the driving. The corresponding classical system is an area-preserving map  $U$ .

We first introduce the fictitious integrable system approach [36]. It is based on a fictitious integrable system  $H_{\text{reg}}(q, p)$ , which resembles the regular region of the mixed system as closely as possible and extends it beyond its boundary, see Fig. 2(c). This allows to decompose the Hilbert space into a regular and a chaotic part: As basis states of these parts we use the eigenstates of  $H_{\text{reg}}$ , which localize on tori with quantized action  $I_m = \frac{1}{2\pi} \oint p(q) dq = \hbar(m + \frac{1}{2})$ . The action  $I_b$  of the boundary torus is used to divide these states into regular basis states  $|I_m\rangle$  with  $I_m < I_b$  and chaotic basis states with  $I_m \geq I_b$ , which will be called  $|I_{\text{ch}}\rangle$  in the following. Here,  $I_b$  is the (not necessarily quantized) action of the first torus of  $H_{\text{reg}}$  that is entirely located in the chaotic region of  $U$ , see Fig. 2. In terms of the time evolution operator  $\hat{U}$  of the mixed system, the rate  $\gamma_m$  of direct regular-to-chaotic tunneling from the  $m$ th quantizing torus to the chaotic region, is determined by summing the transition probabilities to all chaotic basis states [36]

$$\gamma_m = \sum_{\text{ch}} |\langle I_{\text{ch}} | \hat{U} | I_m \rangle|^2. \quad (2)$$

We now evaluate Eq. (2) semiclassically, which will lead to our main result Eq. (6). To this end we express the tunneling matrix elements  $\langle I_{\text{ch}} | \hat{U} | I_m \rangle$  in the basis of the fictitious integrable system by generalizing the time evolution technique of complex paths [28]. Introducing

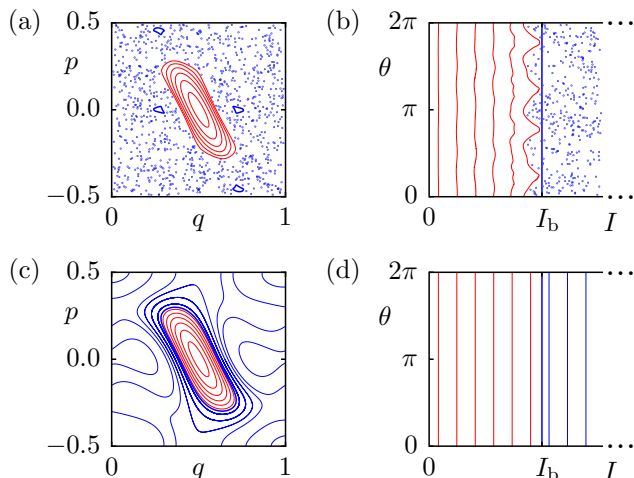


FIG. 2. (color online) (a) Phase space of the standard map at  $\kappa = 2.9$  with regular tori (lines) and a chaotic orbit (dots), (b) in the action-angle coordinates of  $H_{\text{reg}}$ . (c) Phase space of  $H_{\text{reg}}$ , (d) in action-angle coordinates. The boundary torus  $I_b$  is marked by a thick line.

the position representation gives

$$\langle I_{\text{ch}} | \hat{U} | I_m \rangle = \int dq' \int dq \langle I_{\text{ch}} | q' \rangle \langle q' | \hat{U} | q \rangle \langle q | I_m \rangle. \quad (3)$$

Here, the first and the last factor are the initial and the final wave function of  $H_{\text{reg}}$ . These two factors are replaced by their semiclassical counter-parts, using the quantization of canonical transformations for the wave functions [39]. The propagator,  $\langle q' | \hat{U} | q \rangle$ , is also expressed semiclassically [28, 40]. The arising integrals over  $q$  and  $q'$  are evaluated by the method of steepest descent [41], i.e., a saddle-point approximation, which explicitly allows to take complex paths into account. This results in a semiclassical propagator for the tunneling matrix elements

$$\langle I_{\text{ch}} | \hat{U} | I_m \rangle = \sum_{\nu} \sqrt{\frac{\hbar}{2\pi} \frac{\partial^2 \mathcal{S}_{\nu}(I_{\text{ch}}, I_m)}{\partial I_{\text{ch}} \partial I_m}} \exp\left(i \left[ \frac{\mathcal{S}_{\nu}(I_{\text{ch}}, I_m)}{\hbar} + \phi_{\nu} \right]\right). \quad (4)$$

It is constructed from classical paths  $\nu$ , with action  $\mathcal{S}_{\nu}$  and a Maslov-phase shift  $\phi_{\nu}$ . These paths  $\nu$  have to connect the initial torus  $I_m$  to the final torus  $I_{\text{ch}}$ . Since there are no such paths in real phase space, see Fig. 2, the above propagator is exclusively constructed from paths of the complexified phase space. Such a complex path  $\nu$  consists of three segments: (i) The first segment is the curve  $\mathcal{C}_{m,\nu}$  on the analytic continuation of the initial torus  $I_m$  of  $H_{\text{reg}}$  into the complexified phase space. This curve connects the real phase space to a specific point  $(q_{\nu}, p_{\nu})$  whose location is determined by the next segment. (ii) The second segment is the classical path of the complexified mixed system  $U$ . It has to connect  $(q_{\nu}, p_{\nu})$  on the initial complexified torus  $I_m$  to a point  $(q'_{\nu}, p'_{\nu})$  on the final complexified torus  $I_{\text{ch}}$ . This requirement determines the point  $(q_{\nu}, p_{\nu})$  of the first segment. (iii) The final segment is the curve  $\mathcal{C}_{\text{ch},\nu}$  which connects the point  $(q'_{\nu}, p'_{\nu})$  back to the real phase space, along the complexified final torus  $I_{\text{ch}}$  of  $H_{\text{reg}}$ . The three segments are sketched in Fig. 1 (green curves). Their explicit determination for the standard map will be described below.

The action  $\mathcal{S}_{\nu}$  of such complex paths is given by

$$\mathcal{S}_{\nu}(I_{\text{ch}}, I_m) = \int_{\mathcal{C}_{m,\nu}} p(q) dq + \mathcal{S}_{\nu}^U(q_{\nu}, q'_{\nu}) + \int_{\mathcal{C}_{\text{ch},\nu}} p(q) dq. \quad (5)$$

Here, the first and the last contribution are action integrals carried out along the curves  $\mathcal{C}_{m,\nu}$  and  $\mathcal{C}_{\text{ch},\nu}$ , respectively. The action  $\mathcal{S}_{\nu}^U(q_{\nu}, q'_{\nu})$  originates from the second segment, where the mixed system propagates between the initial and the final tori. From the possibly infinite number of paths, which contribute to the sum in Eq. (4), we select the dominant ones having the smallest positive imaginary action. To obtain the relative phase between the paths  $\nu$ , the curves  $\mathcal{C}_{m,\nu}$  have to start at common reference points and the curves  $\mathcal{C}_{\text{ch},\nu}$  have to end at common reference points in real phase space.

In the following we evaluate the tunneling rates in Eq. (2) semiclassically. To this end, we replace the sum  $\sum_{\text{ch}}$  by an integral  $\int_{I_b}^{\infty} dI_{\text{ch}}/\hbar$ , starting from the boundary action  $I_b$ . Here, we exploit that transition matrix elements are semiclassically not restricted to quantizing actions. The matrix elements, Eq. (4), are maximal at the boundary  $I_b$  and decrease exponentially with increasing  $I_{\text{ch}}$ . This allows to approximate the integral asymptotically [41], leading to our final semiclassical result for dynamical tunneling rates

$$\gamma_m = \sum_{\nu} \frac{\hbar}{4\pi} \frac{\left| \frac{\partial^2 \mathcal{S}_{\nu}(I_b, I_m)}{\partial I_b \partial I_m} \right|}{\text{Im} \frac{\partial \mathcal{S}_{\nu}(I_b, I_m)}{\partial I_b}} \exp \left( -\frac{2 \text{Im} \mathcal{S}_{\nu}(I_b, I_m)}{\hbar} \right). \quad (6)$$

Here, the only relevant paths are those which connect the regular action  $I_m$  to the boundary action  $I_b$ . Moreover, it generalizes the familiar WKB-prediction of Eq. (1). The semiclassical approximation leading to Eq. (6) cancels the interference terms between different paths. Hence, it is not necessary to determine the relative phases of the individual paths for a semiclassical prediction of dynamical tunneling rates.

We illustrate our approach and demonstrate its successful predictions by applying it to the standard map [42], which is the paradigmatic example of a mixed system. It is obtained from the one-dimensional kicked Hamiltonian  $H(q, p) = T(p) + V(q) \sum_n \delta(t - n)$  with  $T(p) = p^2/2$  and  $V(q) = \kappa/(2\pi)^2 \cos(2\pi q)$ . The stroboscopic time evolution is given by the map  $U$

$$q' = q + T'(p) \quad p' = p - V'(q'). \quad (7)$$

The quantum time-evolution operator  $\hat{U}$  is given by  $\hat{U} = \exp(-iV(q)/\hbar) \exp(-iT(p)/\hbar)$ , where  $\hbar = 2\pi\hbar$  is the effective Planck constant. We determine the tunneling rate  $\gamma_m$  of the  $m$ th quantizing torus semiclassically, using Eq. (6): One constructs a fictitious integrable system  $H_{\text{reg}}(q, p)$ , Fig. 2(c), based on the frequencies of the main regular island [36]. For this  $H_{\text{reg}}(q, p)$  there is a canonical transformation to action-angle coordinates  $(I, \theta)$ , see Fig. 2(d), giving  $H_{\text{reg}}(I)$ . This allows for searching the complex paths  $\nu$  which connect the real initial torus  $I_m$  and the real boundary torus  $I_b$  of  $H_{\text{reg}}$ , according to steps (i)-(iii). For step (i) the torus  $I_m$  is analytically continued by complexifying the angle  $\theta$ . This torus forms a plane in the complexified phase space, see Fig. 3, parametrized by the real and the imaginary part of the angle  $\theta$ . To obtain the canonical transformation to the corresponding  $(q, p)$ -coordinates, we numerically integrate Hamilton's equations for  $H_{\text{reg}}(q, p)$  in imaginary time, starting from the real torus  $I_m$ . The integration is done up to time  $t = i\text{Im}(\theta)/\omega_m$  where  $\omega_m$  is the frequency of the real torus  $I_m$ . For step (ii) the points  $(q, p)$  of the complexified initial torus  $I_m$  are mapped by the complexification of the standard map, Eq. (7), to points  $(q', p')$ . The points  $(q, p)$  are mapped onto the complexified torus  $I_b$ , only if the energy  $E' = H_{\text{reg}}(q', p')$

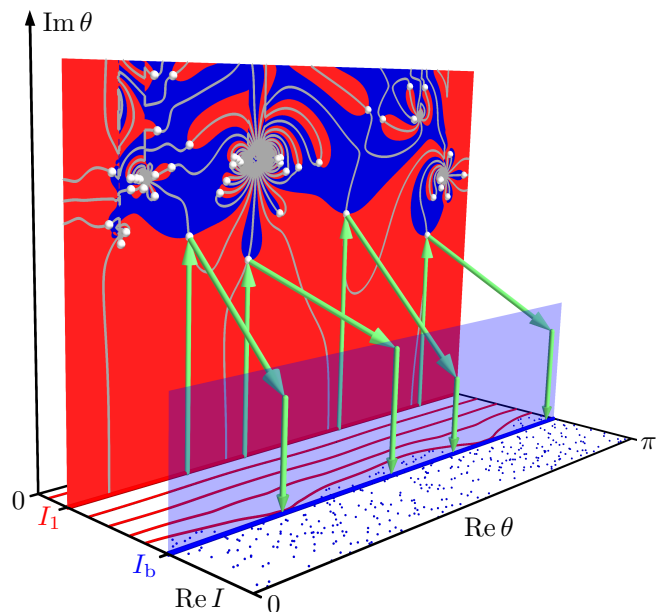


FIG. 3. (color online) Dominant complex paths (green arrows) for the tunneling rate  $\gamma_1$  of the standard map at  $\kappa = 2.9$  and  $\hbar = 1/50$  as in Fig. 1 but in action-angle representation. The planes are the complexifications of the initial torus  $I_1$  and the final torus  $I_b$  of  $H_{\text{reg}}$ . White dots represent points on  $I_1$  which map onto  $I_b$ . They are at the intersection of the gray lines ( $\text{Im} E' = 0$ ) with the boundary between light red regions ( $\text{Re} E' < E_b$ ) and dark blue regions ( $\text{Re} E' > E_b$ ). The visualization is simplified by shifting the angle of the endpoints of step (ii) by  $-\omega_b$  along  $I_b$  [as also done in Fig. 1].

equals the energy  $E_b$  of the boundary torus  $I_b$ . These numerically determined points are labeled  $(q_\nu, p_\nu)$  and are shown in Fig. 3 as white dots. For step (iii) we integrate Hamilton's equations for  $H_{\text{reg}}$  in negative imaginary time to get back to the real torus  $I_b$ . Combining the three steps (i)-(iii) gives the complex paths  $\nu$ . Finally we evaluate the action of these paths  $\nu$  according to Eq. (5) in which the second contribution for the standard map is given by [43, 44]

$$\mathcal{S}^U(q_\nu, q'_\nu) = \frac{(q_\nu - q'_\nu)^2}{2} - V(q'_\nu). \quad (8)$$

From the infinite number of paths  $\nu$  contributing to the sum in Eq. (6) we select the dominant ones, which have the smallest positive imaginary action, see arrows in Fig. 3. There, the four paths  $\nu$  (together with their symmetry partners) contribute 20 %, 6 %, 33 %, and 41 % (left to right) to the tunneling rate  $\gamma_1$ . Note, that we account for the parity of the standard map by just considering one symmetry partner and doubling its contribution in Eq. (4), which leads to an additional factor of four in Eq. (6).

The semiclassically predicted tunneling rates  $\gamma_m$ , Eq. (6), for the standard map are shown as lines in Fig. 4. Numerically determined tunneling rates (dots) are ob-

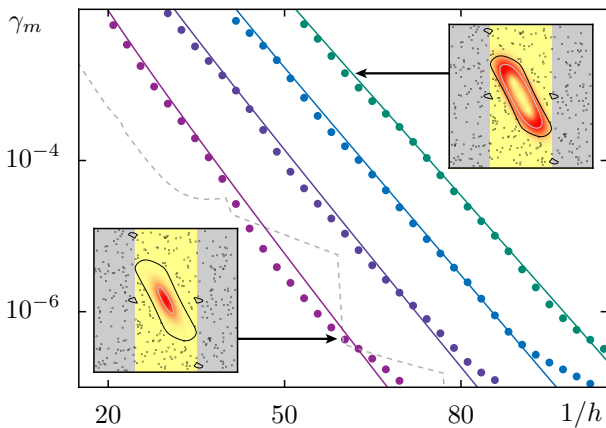


FIG. 4. (color online) Tunneling rates  $\gamma_m$  of the standard map at  $\kappa = 2.9$  for  $m = 0, 1, 2, 3$  vs.  $1/h$ . The semiclassical prediction, Eq. (6), (straight lines) is compared to numerical rates (dots) and for  $m = 0$  to the quantum evaluation of Eq. (2) (dashed line). The insets show the Husimi representation of the eigenstates with  $m = 0$  and  $m = 3$  at  $h = 1/60$  and the corresponding quantizing tori (gray lines) in phase space with absorbing regions (gray).

tained by opening the system [36] tangential to the regular region (inset in Fig. 4), which is consistent with the choice of  $I_b$  (Fig. 2). The semiclassical prediction accurately describes the numerical tunneling rates, with deviations by less than a factor of 2. This considerably improves the quality of previous predictions [36], in which one finds quantization steps from the quantum mechanical evaluation of Eq. (2), see Fig. 4. These quantization steps do not occur in the semiclassical evaluation, as  $I_b$  does not have to obey any quantization condition. The small deviations at small  $\gamma$  can be attributed to nonlinear resonances. One should be able to take this effect into account, by taking our semiclassical prediction for direct regular-to-chaotic tunneling and combine [37] it with resonance-assisted tunneling.

We now make a couple of remarks: (a) Our complex-path approach also works for other parameters  $\kappa$  of the standard map, leading to predictions of similar quality. Deviations due to nonlinear resonances may arise at

larger  $\gamma$  already. (b) Partial barriers which limit transport in the chaotic region can additionally suppress dynamical tunneling [26]. This effect is not yet considered in our investigations since we open the system at the boundary of the regular region. (c) We obtain the tunneling rates  $\gamma_m$  from semiclassical propagation over a single time step and find that only a small number of complex paths  $\nu$  contribute to Eq. (6). Thus the determination of tunneling rates turns out to be considerably simpler than the semiclassical propagation of wave packets over long times, for which a careful selection among hundreds of dominant paths is needed [28]. (d) The natural boundary [45, 46] makes it impossible to continue regular tori of non-integrable systems deep into the complexified phase space [12, 14, 29]. We overcome this problem by complexifying the tori of the fictitious integrable system  $H_{\text{reg}}$ . (e) The choice of  $H_{\text{reg}}$  is not unique and defining a precise classical criterion for its quality is an open question. While the paths  $\nu$  may depend on this choice, we expect to obtain a prediction of tunneling rates  $\gamma_m$  with similar agreement to numerical rates. (f) Determining tunneling rates just from WKB-paths along the initial torus  $I_m$  of  $H_{\text{reg}}$ , which was successful in specific situations [30, 33, 34, 36], gives for the standard map a rough estimate only.

In summary, we have presented a complex-path approach which allows for predicting regular-to-chaotic tunneling rates in systems with a mixed phase space. We have successfully applied this method to predict tunneling rates of the standard map. For the future it is desirable to develop a complete semiclassical description of regular-to-chaotic tunneling even in the presence of resonance-assisted tunneling. Moreover, the application of our approach to higher dimensional systems like billiards, optical microcavities, or atoms and molecules remains an open problem. Finally, we believe that our approach is the basis to reveal the universal classical properties which govern dynamical tunneling.

We acknowledge helpful discussions with S. Creagh and K. Ikeda and the participants of the Advanced Study Group "Towards a Semiclassical Theory of Dynamical Tunneling". We thank the DFG for support within Forschergruppe 760 "Scattering Systems with Complex Dynamics". AB thanks the Japan Society for the Promotion of Science for supporting his stay in Japan.

[1] L. D. Landau and E. M. Lifshitz, *Course of Theoretical Physics, Vol.3: Quantum Mechanics* (Pergamon Press, New York, 1991).  
 [2] E. Merzbacher, *Quantum mechanics* (Wiley, New York, 1998).  
 [3] M. V. Berry and K. E. Mount, Rep. Proc. Phys. **35**, 315 (1972).  
 [4] S. C. Creagh, J. Phys. A. **27**, 4969 (1994).  
 [5] J. Zakrzewski, D. Delande, and A. Buchleitner, Phys. Rev. E **57**, 1458 (1998).

[6] A. Buchleitner, D. Delande, and J. Zakrzewski, Phys. Rep. **368**, 409 (2002).  
 [7] S. Wimberger, P. Schlagheck, C. Eltschka, and A. Buchleitner, Phys. Rev. Lett. **97**, 043001 (2006).  
 [8] W. K. Hensinger, H. Häffner, A. Browaeys, N. R. Heckenberg, K. Helmerson, C. McKenzie, G. J. Millburn, W. D. Phillips, S. L. Rolston, H. Rubinsztein-Dunlop, et al., Nature **412**, 52 (2001).  
 [9] D. A. Steck, W. H. Oskay, and M. G. Raizen, Science **293**, 274 (2001).



- [10] C. Dembowski, H.-D. Gräf, A. Heine, R. Hofferbert, H. Rehfeld, and A. Richter, *Phys. Rev. Lett.* **84**, 867 (2000).
- [11] A. Bäcker, R. Ketzmerick, S. Löck, M. Robnik, G. Vidmar, R. Höhmann, U. Kuhl, and H.-J. Stöckmann, *Phys. Rev. Lett.* **100**, 174103 (2008).
- [12] S. C. Creagh, *Phys. Rev. Lett.* **98**, 153901 (2007).
- [13] A. Bäcker, R. Ketzmerick, S. Löck, J. Wiersig, and M. Hentschel, *Phys. Rev. A* **79**, 063804 (2009).
- [14] S. C. Creagh and M. M. White, *Phys. Rev. E* **85**, 015201 (2012).
- [15] J. Feist, A. Bäcker, R. Ketzmerick, S. Rotter, B. Huckestein, and J. Burgdörfer, *Phys. Rev. Lett.* **97**, 116804 (2006); J. Feist, A. Bäcker, R. Ketzmerick, J. Burgdörfer, and S. Rotter, *Phys. Rev. B* **80**, 245322 (2009).
- [16] M. J. Davis and E. J. Heller, *J. Chem. Phys.* **75**, 246 (1981).
- [17] S. Keshavamurthy and P. Schlagheck, *Dynamical Tunneling: Theory and Experiment* (CRC Press, New York, 2011).
- [18] L. Hufnagel, R. Ketzmerick, M.-F. Otto, and H. Schanz, *Phys. Rev. Lett.* **89**, 154101 (2002).
- [19] A. Bäcker, R. Ketzmerick, and A. G. Monastera, *Phys. Rev. Lett.* **94**, 054102 (2005); *Phys. Rev. E* **75**, 066204 (2007).
- [20] G. Vidmar, H.-J. Stöckmann, M. Robnik, U. Kuhl, R. Höhmann, and S. Grossmann, *J. Phys. A* **40**, 13883 (2007).
- [21] B. Batistić and M. Robnik, *J. Phys. A* **43**, 215101 (2010).
- [22] A. Bäcker, R. Ketzmerick, S. Löck, and N. Mertig, *Phys. Rev. Lett.* **106**, 024101 (2011).
- [23] T. Rudolf, N. Mertig, S. Löck, and A. Bäcker, *Phys. Rev. E* **85**, 036213 (2012).
- [24] J. D. Hanson, E. Ott, and T. M. Antonsen, *Phys. Rev. A* **29**, 819 (1984).
- [25] M. Wilkinson, *Physica D* **21**, 341 (1986).
- [26] O. Bohigas, S. Tomsovic, and D. Ullmo, *Phys. Rep.* **223**, 43 (1993).
- [27] S. Tomsovic and D. Ullmo, *Phys. Rev. E* **50**, 145 (1994).
- [28] A. Shudo and K. S. Ikeda, *Phys. Rev. Lett.* **74**, 682 (1995); *Physica D* **115**, 234 (1998).
- [29] S. C. Creagh, *Tunneling in two dimensions*, in *Tunneling in Complex Systems* (World Scientific, Singapore, 1998).
- [30] O. Brodier, P. Schlagheck, and D. Ullmo, *Phys. Rev. Lett.* **87**, 064101 (2001); *Ann. of Phys.* **300**, 88 (2002).
- [31] V. A. Podolskiy and E. E. Narimanov, *Phys. Rev. Lett.* **91**, 263601 (2003).
- [32] C. Eltschka and P. Schlagheck, *Phys. Rev. Lett.* **94**, 014101 (2005).
- [33] M. Sheinman, S. Fishman, I. Guarneri, and L. Rebuzzini, *Phys. Rev. A* **73**, 052110 (2006).
- [34] A. Mouchet, *J. Phys. A* **40**, F663 (2007).
- [35] A. Shudo, Y. Ishii, and K. S. Ikeda, *J. Phys. A* **35**, L225 (2002); *Europhys. Lett.* **81**, 50003 (2008); *J. Phys. A* **42**, 265101 (2009); *J. Phys. A* **42**, 265102 (2009).
- [36] A. Bäcker, R. Ketzmerick, S. Löck, and L. Schilling, *Phys. Rev. Lett.* **100**, 104101 (2008); A. Bäcker, R. Ketzmerick, and S. Löck, *Phys. Rev. E* **82**, 056208 (2010).
- [37] S. Löck, A. Bäcker, R. Ketzmerick, and P. Schlagheck, *Phys. Rev. Lett.* **104**, 114101 (2010).
- [38] J. Le Deunff and A. Mouchet, *Phys. Rev. E* **81**, 046205 (2010).
- [39] W. H. Miller, *Adv. Chem. Phys.* **25**, 66 (1974).
- [40] L. S. Schulman, *Techniques and Applications of Path Integration* (Dover, Minola, New York, 2005).
- [41] J. D. Murray, *Asymptotic analysis* (Clarendon Press, Oxford, 1974).
- [42] B. V. Chirikov, *Phys. Rep.* **52**, 263 (1979).
- [43] M. V. Berry, N. L. Balzas, M. Tabor, and A. Voros, *Ann. of Phys.* **122**, 26 (1979).
- [44] E. B. Bogomolny, *Nonlinearity* **5**, 805 (1992).
- [45] J. M. Greene and I. C. Percival, *Physica D* **3**, 530 (1981).
- [46] I. C. Percival, *Physica D* **6**, 67 (1982).